

## PROPERTIES OF GALAXY DARK MATTER HALOS FROM WEAK LENSING

HENK HOEKSTRA<sup>1,2,3</sup>, H.K.C. YEE<sup>2,3</sup>, AND MICHAEL D. GLADDERS<sup>3,4</sup>*Draft version October 31, 2018*

## ABSTRACT

We present the results of a study of weak lensing by galaxies based on 45.5 deg<sup>2</sup> of  $R_C$  band imaging data from the Red-Sequence Cluster Survey (RCS). We define a sample of lenses with  $19.5 < R_C < 21$ , and a sample of background galaxies with  $21.5 < R_C < 24$ .

We present the first weak lensing detection of the flattening of galaxy dark matter halos. We use a simple model in which the ellipticity of the halo is  $f$  times the observed ellipticity of the lens. We find a best fit value of  $f = 0.77_{-0.21}^{+0.18}$ , suggesting that the dark matter halos are somewhat rounder than the light distribution. The fact that we detect a significant flattening implies that the halos are well aligned with the light distribution. Given the average ellipticity of the lenses, this implies a halo ellipticity of  $\langle e_{\text{halo}} \rangle = 0.33_{-0.09}^{+0.07}$ , in fair agreement with results from numerical simulations of CDM. We note that this result is formally a lower limit to the flattening, since the measurements imply a larger flattening if the halos are not aligned with the light distribution. Alternative theories of gravity (without dark matter) predict an isotropic lensing signal, which is excluded with 99.5% confidence. Hence, our results provide strong support for the existence of dark matter.

We also study the average mass profile around the lenses, using a maximum likelihood analysis. We consider two models for the halo mass profile: a truncated isothermal sphere (TIS) and an NFW profile. We adopt observationally motivated scaling relations between the lens luminosity and the velocity dispersion and the extent of the halo. The TIS model yields a best fit velocity dispersion of  $\sigma = 136 \pm 5 \pm 3$  km/s (all errors are 68% confidence limits; the first error bar indicates the statistical uncertainty, whereas the second error bar indicates the systematic error) and a truncation radius  $s = 185_{-28}^{+30} h^{-1}$  kpc for a galaxy with a fiducial luminosity of  $L_B = 10^{10} h^{-2} L_{B\odot}$  (under the assumption that the luminosity does not evolve with redshift). Alternatively, the best fit NFW model yields a mass  $M_{200} = (8.4 \pm 0.7 \pm 0.4) \times 10^{11} h^{-1} M_{\odot}$  and a scale radius  $r_s = 16.2_{-2.9}^{+3.6} h^{-1}$  kpc. This value for the scale radius is in excellent agreement with predictions from numerical simulations for a halo of this mass.

*Subject headings:* cosmology: observations – dark matter – gravitational lensing – galaxies: haloes

## 1. INTRODUCTION

The existence of massive dark matter halos around galaxies is widely accepted, based on different lines of evidence, such as flat rotation curves of spiral galaxies (e.g., Van Albada & Sancisi 1986) and strong lensing systems (e.g., Keeton, Kochanek & Falco 1998). However, relatively little is known about the properties of dark matter halos. Strong lensing only probes the gravitational potential on small (projected) scales, whereas the lack of visible tracers at large radii hamper dynamical methods. To date, only satellite galaxies have provided some information (e.g., Zaritsky & White 1994; McKay et al. 2002; Prada et al. 2003).

A promising approach to study the galaxy dark matter halos is weak gravitational lensing. The tidal gravitational field of the dark matter halo introduces small coherent distortions in the images of distant background galaxies. The weak lensing signal can be measured out to large projected distances from the lens, and hence provides a unique

probe of the gravitational potential on large scales.

The applications of this approach are numerous: one can infer masses of galaxies and compare the results to their luminosities (e.g., McKay et al. 2001; Wilson et al. 2001), or one can attempt to constrain the halo mass profile (e.g., Brainerd et al. 1996; Hudson et al. 1998; Fischer et al. 2000; Hoekstra et al. 2003). Also, weak lensing can be used to constrain the shapes of halos by measuring the azimuthal variation of the lensing signal. Unfortunately, one can only study ensemble averaged properties, because the weak lensing signal induced by an individual galaxy is too low to be detected.

A successful measurement of the lensing signal requires large samples of both lenses and background galaxies. The first attempt to detect the lensing signal by galaxies was made by Tyson et al. (1984) using photographic plates. It took more than a decade and CCD cameras before the first detections were reported (Brainerd et al. 1996; Griffiths et al. 1996; Dell’Antonio & Tyson 1996; Hudson et al. 1998). These early results were limited by the small areas covered by the observations.

The accuracy with which the galaxy-galaxy lensing signal can be measured depends on the area of sky that is observed, and on the availability of redshifts for the lenses (as it allows for a proper scaling of the lensing signal). Photometric redshifts were used by Hudson et al. (1998) to scale the lensing signal of galaxies in the Hubble Deep

<sup>1</sup> CITA, University of Toronto, Toronto, Ontario M5S 3H8, Canada

<sup>2</sup> Department of Astronomy, University of Toronto, Toronto, Ontario M5S 3H8, Canada

<sup>3</sup> Visiting Astronomer, Canada-France-Hawaii Telescope, which is operated by the National Research Council of Canada, Le Centre National de Recherche Scientifique, and the University of Hawaii

<sup>4</sup> Observatories of the Carnegie Institution of Washington, 813 Santa Barbara Street, Pasadena, California 91101

Field, and by Wilson et al. (2001) who measured the lensing signal around early type galaxies as a function of redshift. Furthermore, several lensing studies targeted regions covered by redshift surveys. Smith et al. (2001) used 790 lenses from the Las Campanas Redshift Survey; Hoekstra et al. (2003) used 1125 lenses from the Canadian Network for Observational Cosmology Field Galaxy Redshift Survey (CNOC2). The areas covered by these surveys are relatively small.

The Sloan Digital Sky Survey (SDSS) combines both survey area and redshift information. Its usefulness for galaxy-galaxy lensing was demonstrated clearly by Fischer et al. (2000). More recently, McKay et al. (2001) used the available SDSS redshift information to study the galaxy-galaxy lensing signal as a function of galaxy properties (also see Guzik & Seljak 2002; Seljak 2002).

The data used in this paper currently lacks redshift information for the lenses. However, compared to previous work, the combination of large area and depth of our observations allow us to measure the galaxy lensing signal with great precision. We use  $45.5 \text{ deg}^2$  of  $R_C$ -band imaging data from the Red-Sequence Cluster Survey (RCS). These data have been used previously for several weak lensing studies. Hoekstra et al. (2002a; 2002b) placed joint constraints on  $\Omega_m$  and  $\sigma_8$  by measuring the lensing signal caused by large scale structure. Related to the subject of this paper is the study of the bias parameters as a function of scale by Hoekstra et al. (2001b) and Hoekstra et al. (2002c). The latter studies made use of the galaxy-mass cross-correlation function measured from the RCS data. Here we use the galaxy-mass cross-correlation function for a different purpose: we effectively deconvolve the cross-correlation function to study the properties of dark matter halos surrounding galaxies at intermediate redshifts.

The structure of the paper is as follows. In §2 we briefly discuss the data and the redshift distributions of the lenses and the sources. The ensemble averaged tangential shear around the lenses (galaxy-mass cross-correlation function) is presented in §3. In §4 we use a maximum likelihood analysis to derive constraints on the extent of dark matter halos. The measurement of the projected shapes of the halos is presented in §5.

## 2. OBSERVATIONS AND ANALYSIS

We use the  $R_C$ -band imaging data from the Red-Sequence Cluster Survey (Yee & Gladders 2001; Gladders & Yee 2003). The complete survey covers  $90 \text{ deg}^2$  in both  $R_C$  and  $z'$ , spread over 22 widely separated patches of  $\sim 2.1 \times 2.3$  degrees. In this paper we use data from the northern half of the survey, which consists of 10 patches, observed with the CFH12k camera on the CFHT. These data cover  $45.5 \text{ deg}^2$  on the sky, but because of masking the effective area is somewhat smaller. In the lensing analysis we use a total of  $42 \text{ deg}^2$ . A detailed description of the data reduction and object analysis can be found in Hoekstra et al. (2002a), to which we refer for technical details. Here we present a short description of the various steps in the analysis.

We use single exposures in our analysis, and consequently cosmic rays have not been removed. However, cosmic rays are readily eliminated from the photometric catalogs: small, but very significant objects are likely to

be cosmic rays, or artifacts from the CCD. The object finder gives fair estimates of the object sizes, and we remove all objects smaller than the size of the PSF. Some faint cosmic rays may hit galaxies, and consequently might not be recognized as cosmic rays. Based on the number of cosmic ray hits, and the area covered by galaxies we find that less than 0.2% of the galaxies might be affected. Also, cosmic rays only introduce additional noise in the shape measurement, but do not bias the result. Consequently we conclude that remaining cosmic rays have a negligible effect on our results.

The objects in this cleaned catalog are then analysed, which yield estimates for the size, apparent magnitude, and shape parameters (polarisation and polarisabilities). The objects in this catalog are inspected by eye, in order to remove spurious detections. These objects have to be removed because their shape measurements are affected by cosmetic defects (such as dead columns, bleeding stars, halos, diffraction spikes) or because the objects are likely to be part of a resolved galaxy (e.g., HII regions).

To measure the small, lensing induced distortions in the images of the faint galaxies it is important to accurately correct the shapes for observational effects, such as PSF anisotropy, seeing and camera shear; PSF anisotropy can mimic a cosmic shear signal, and a correction for the seeing is required to relate the measured shapes to the real lensing signal. To do so, we follow the procedure outlined in Hoekstra et al. (1998). We select a sample of moderately bright stars from our observations, and use these to characterize the PSF anisotropy and seeing. We fit a second order polynomial to the shape parameters of the selected stars for each chip of the CFH12k camera. These results are used to correct the shapes of the galaxies for PSF anisotropy and seeing.

The effect of the PSF is not the only observational distortion that has to be corrected. The optics of the camera stretches the images of galaxies (i.e., it introduces a shear) because of the non-linear remapping of the sky onto the CCD. We have used observations of astrometric fields to find the mapping between the sky and the CCD pixel coordinate system, and derived the corresponding camera shear, which is subsequently subtracted from the galaxy ellipticity (see Hoekstra et al. 1998).

The findings presented in Hoekstra et al. (2002a) suggest that the correction for PSF anisotropy has worked well. The absence of a “B”-mode on large scales in the measurements of the cosmic shear (Hoekstra et al. 2002b) provides additional evidence that systematics are well under control (the small scale “B”-mode is attributed to intrinsic alignments). Furthermore, cosmic shear studies are much more sensitive to systematics than galaxy-galaxy lensing measurements (e.g., see Hoekstra et al. 2003). In galaxy-galaxy lensing one measures the lensing signal that is perpendicular to the lines connecting many lens-source pairs. These connecting lines are randomly oriented with respect to the PSF anisotropy, and hence suppress any residual systematics.

### 2.1. Redshift distributions

For the analysis presented here, we select a sample of “lenses” and “sources” on the basis of their apparent  $R_C$  magnitude. We define galaxies with  $19.5 < R_C < 21$

as lenses, and galaxies with  $21.5 < R_C < 24$  as sources which are used to measure the lensing signal. This selection yields a sample of  $\sim 1.2 \times 10^5$  lenses and  $\sim 1.5 \times 10^6$  sources.

For a singular isothermal sphere, the amplitude of the lensing signal depends on  $\langle\beta\rangle$ , the average ratio of the angular diameter distances between the lens and the source,  $D_{ls}$ , and the distance between the observer and the source  $D_s$ . More general, the signal also depends on  $D_l$ , the distance between the observer and the lens. Hence, to interpret the measurements, such as size and mass, one needs to know the redshift distributions of both lenses and sources.

The CNOC2 Field Galaxy Redshift Survey (e.g., Lin et al. 1999; Yee et al. 2000; Carlberg et al. 2001) has measured the redshift distribution of field galaxies down to  $R_C = 21.5$ , which is ideal, given our limits of  $19.5 < R_C < 21$ . The derived redshift distribution gives a median redshift  $z = 0.35$  for the lens sample. In addition, we use the redshifts and the colors of the galaxies observed in the CNOC2 survey to compute their rest-frame  $B$  luminosity.

Compared to studies using SDSS data (McKay et al. 2001) we have the disadvantage that we do not have (spectroscopic) redshifts for the individual lenses. As shown by Schneider & Rix (1997) and Hoekstra et al. (2003) this limits the accuracy of the measurements. We can derive useful constraints on the masses and extent of dark matter halos, but we have to assume scaling relations between these parameters and the luminosity of the galaxies. Multi-color data for the northern part of the RCS will be available in the near future, allowing us to select a sample of lenses based on their photometric redshifts, and constrain the scaling relations.

Nevertheless, the large area covered by the RCS allows us to derive interesting information about the properties of the lenses. In §4 we use different cuts in apparent magnitude to study the properties of dark matter halos using a maximum likelihood analysis.

For the source galaxies the situation is more complicated. These galaxies are generally too faint for spectroscopic surveys, although recently Cohen et al. (2000) measured spectroscopic redshifts around the Hubble Deep Field North down to  $R_C \sim 24$ . Cohen et al. (2000) find that the spectroscopic redshifts agree well with the photometric redshifts derived from multi-color photometry. Because of likely field-to-field variations in the redshift distribution, we prefer to use the photometric redshift distributions derived from both Hubble Deep Fields (Fernández-Soto et al. 1999), which yields a median redshift of  $z = 0.53$  for the source galaxies.

The adopted source and lens redshift distributions result in an average value of  $\langle\beta\rangle = 0.29 \pm 0.01$  (average for the full sample of lenses and sources), where the error bar is based on the field-to-field variation and the finite number of galaxies in the Hubble Deep Fields. The uncertainty in  $\langle\beta\rangle$  affects predominantly our estimates for the galaxy masses (and velocity dispersions), but is negligible for the other model parameters. We note that for the galaxy-galaxy lensing analysis presented here the relevant parameter is  $\langle L_B^{0.3}\beta\rangle$ , as opposed to simply  $\langle\beta\rangle$ , but we have verified that results in a negligible change in the adopted systematic error. Throughout the paper we indicate the

systematic error in the masses and velocity dispersions by a second error bar.

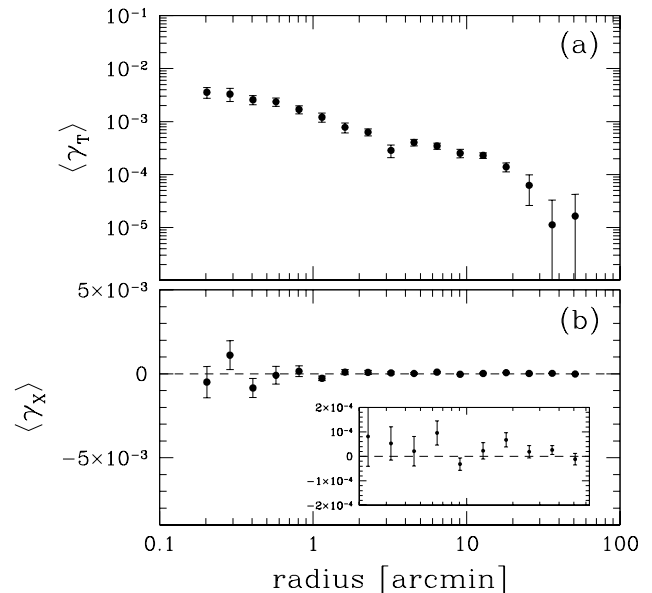


FIG. 1.— (a) The galaxy-mass cross-correlation function as a function of angular scale. The lenses are selected on the basis of their apparent  $R_C$ -band magnitude, taking  $19.5 < R_C < 21$ . The tangential alignment is detected out to a radius of 1 degree. The signal on these large scale no longer reflects the mass of the lens, but the clustering properties of the lenses. (b) The signal when the phase of the shear is increased by  $\pi/4$ . No signal should be present if the signal detected in panel (a) is caused by gravitational lensing. The results are consistent with no signal. The error bars are so small that we expanded the y-axis by a factor 25 in the inset of panel (b). The complex geometry of the survey on large scales (holes in the survey area because of masking) results in non-vanishing values of  $\gamma_X$ . Despite these complications, the residuals are remarkably small.

### 3. GALAXY-MASS CROSS-CORRELATION FUNCTION

The galaxy-mass cross-correlation function provides a convenient way to present the measurements. It is obtained from the data by measuring the tangential alignment of the source galaxies with respect to the lens as a function of radius. Its use for studying the halos of galaxies is limited, because the clustering of galaxies complicates a direct interpretation of the signal: on small scales the signal is dominated by the mass distribution of the lens, but on larger scales one measures the superposition of the contributions from many lenses.

The observed galaxy-mass cross-correlation function as a function of angular scale is presented in Figure 1a. A significant signal is detected out to one degree from the lens. If the signal presented in Figure 1a is caused by gravitational lensing, no signal should be present when the phase of the distortion is increased by  $\pi/4$  (i.e., when the sources are rotated by 45 degrees). The results of this test, shown in Figure 1b, suggest that residual systematics are negligible.

Before we can interpret the results we need to examine the contribution of foreground galaxies. Some of the source galaxies will be in front of the lenses, and lower the lensing signal independent of radius. This is absorbed in

the value of  $\langle\beta\rangle$ . These galaxies decrease the lensing signal independent of angular scale. Some sources, however, are physically associated with the lenses. These galaxies cluster around the lenses, affecting the lensing signal more on small scales. We need to account for this source of contamination. To do so, we measure a fractional excess of sources around lenses which decreases with radius as  $f_{\text{bg}}(r) = 0.93r^{-0.76}$  ( $r$  in arcseconds), similar to what was found by Fischer et al. (2000). Under the assumption that the orientations of these galaxies are random (the tidal interaction with the lens has not introduced an additional tangential or radial alignment), the observed lensing signal has to be increased by a factor  $1 + f_{\text{bg}}(r)$ . This assumption is supported by the findings of Bernstein & Norberg (2002) who examined the tangential alignment of satellite galaxies around galaxies, extracted from the 2dF Galaxy Redshift Survey. The measurements presented in Figures 1 have been corrected for this decrease in signal. We note that the correction for the presence of satellite galaxies is small, and has no significant effect on our results.

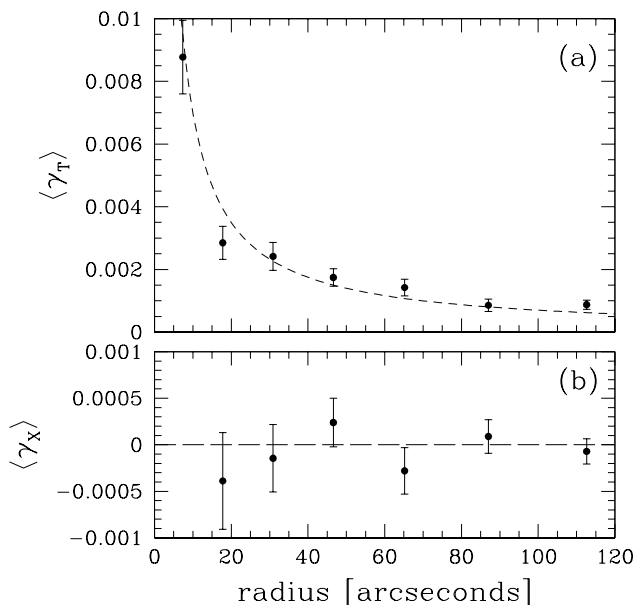


FIG. 2.— (a) Ensemble averaged tangential shear as a function of radius out to 2 arcminutes from the lens. The solid line corresponds to the best fit SIS model to the data at radii smaller than 2 arcminutes. (b) The signal when the phase of the shear is increased by  $\pi/4$ . Note the different vertical scale between panels a and b.

The signal on small angular scales is dominated by a single lens galaxy, and can be used to obtain an estimate of the mass weighted velocity dispersion of the sample of lenses (although such a mass estimate can still be slightly biased because of the clustering of the lenses). Figure 2a shows the ensemble averaged tangential shear on small scales. The measurements presented in Figure 2b show no evidence for residual systematics.

We fit a singular isothermal sphere (SIS) model to the tangential shear at radii smaller than 2 arcminutes (which corresponds to  $\sim 350h^{-1}$  kpc at the mean redshift of the lenses). The best fit model is indicated by the dashed line in Figure 2a. For the Einstein radius  $r_E$  we obtain a value of  $\langle r_E \rangle = 0''.140 \pm 0''.009$ . If we extend the fit to much larger

radii, the inferred value for the Einstein radius increases systematically. With our adopted redshift distributions for the lenses and the sources, the value of  $r_E$  corresponds to a value of  $\langle\sigma^2\rangle^{1/2} = 128 \pm 4$  km/s. The corresponding circular velocity can be obtained using  $V_c = \sqrt{2}\sigma$  (for a spherical halo). The derived value of  $\langle\sigma^2\rangle^{1/2}$  depends on the selection of the sample of lens galaxies, which hampers a direct comparison with other studies.

It is more useful to compute the velocity dispersion of a galaxy with some fiducial luminosity, for which we take  $L_B = 10^{10}h^{-2}L_{B\odot}$ . To do so, we have to adopt a scaling relation between the velocity dispersion and the luminosity. We assume  $\sigma \propto L_B^{0.3}$  (see §4). Furthermore, the luminosity might evolve with redshift, and we will consider two cases. Under the assumption that the luminosity does not evolve with redshift, we obtain a velocity dispersion  $\sigma = 140 \pm 4 \pm 3$  km/s for a galaxy with  $L_B = 10^{10}h^{-2}L_{B\odot}$ . Hoekstra et al. (2003) measured  $\sigma = 115_{-17}^{+15}$  km/s for a galaxy with a luminosity of  $5.6 \times 10^9 h^{-2}L_{B\odot}$  using a sample of galaxies with redshifts from CNOC2. Scaling our measurements to this luminosity implies a velocity dispersion of  $118 \pm 4 \pm 2$  km/s, in excellent agreement with Hoekstra et al. (2003). If we assume that the luminosity scales with redshift as  $L_B \propto (1+z)$ , we find a velocity dispersion of  $\sigma = 150 \pm 4 \pm 3$  km/s for a galaxy with  $L_B(z=0) = 10^{10}h^{-2}L_{B\odot}$ .

#### 4. PROPERTIES OF DARK MATTER HALOS

The galaxy-mass cross-correlation function is the convolution of the galaxy distribution and the galaxy dark matter profiles. To examine the ensemble average properties of the dark matter halos properly, we need to deconvolve the galaxy-mass cross-correlation function (i.e., we need to account for the clustering of the lenses). This is done naturally in a maximum likelihood analysis, where a model for the mass distribution of individual galaxies is compared to the observations.

Fisher et al. (2000) and McKay et al. (2001) used a model with the velocity dispersion and “extent” of the halo as free parameters, and computed the resulting galaxy-mass correlation function for a range of model parameters and compared the results to the observed galaxy-mass correlation function. They obtained good constraints for the velocity dispersion, but were not able to constrain the extent of the dark matter halos.

The galaxy-mass correlation function ignores additional information contained in the data, whereas the maximum likelihood analysis allows one to gauge how much signal might arise from nearby galaxies. Hoekstra et al. (2003) compared their mass model to the observed polarisation field, making use of both components of the polarisation (also see Brainerd et al. 1996; Schneider & Rix 1997; Hudson et al. 1998). This greatly improved the constraints on the extent of the halo, and we will use the same method here.

In our analysis we make an important assumption: all clustered matter is associated with the lenses. If the matter in galaxy groups (or clusters) is associated with the halos of the group members (i.e., the halos are indistinguishable from the halos of isolated galaxies) our results should give a fair estimate of the extent of galaxy halos. However, if a significant fraction of the dark matter is dis-

tributed in common halos, a simple interpretation of the results becomes more difficult.

Hoekstra et al. (2003) examined how known groups in their observed fields affected the lensing results, and found that the masses and sizes might be overestimated by at most  $\sim 10\%$ . Guzik & Seljak (2002) found similar results from their analysis of the galaxy-galaxy lensing signal in the context of halo models. Their approach allows one to separate the contribution from groups to the lensing signal. As expected, Guzik & Seljak (2002) found that the effect depends on galaxy type: early type galaxies are found in high density regions, and are affected more. Alternatively, a comparison with numerical simulations which include a prescription for galaxy formation (e.g., Kauffmann et al. 1999a, 1999b; Guzik & Seljak 2001) can be used to quantify this effect.

Another complication is the fact that we cannot separate the lenses in different morphology classes with the current data. Early and late type galaxies of a given luminosity have different masses, etc. (e.g., Guzik & Seljak 2002). Hence, it is important to keep in mind that the results presented here are ensemble averages over all galaxy types. This is where the SDSS can play an important role, although we can significantly improve the RCS results with upcoming multi-color data.

The variance in the polarisations is approximately constant with apparent magnitude and we approximate the distribution by a Gaussian distribution. With the latter assumption, the log-likelihood follows a  $\chi^2$  distribution with the number of degrees of freedom equal to the number of free model parameters, and the determination of confidence intervals is straightforward. The log-likelihood is given by the sum over the two components of the polarisation  $e_i$  of all the source galaxies

$$\log \mathcal{L} = - \sum_{i,j} \left( \frac{e_{i,j} - P_j^\gamma g_{i,j}^{\text{model}}}{\sigma_{e_j}} \right)^2, \quad (1)$$

where  $g_{i,j}$  are the model distortions,  $P_j^\gamma$  is the shear polarisability,  $e_{i,j}$  are the observed image polarisations for the  $j$ th galaxy, and  $\sigma_{e_j}$  is the dispersion in the polarisation of the  $j$ th galaxy (which is the combination of the intrinsic shape of the galaxy and the measurement error caused by shot noise in the images). In order to minimize the contribution of the baryonic (stellar) component of the galaxies we compare our model to the observations at radii larger than 10 arcseconds (which corresponds to  $\sim 30h^{-1}$  kpc at the redshift of the lenses), where the dark matter halo should dominate the lensing signal.

In our maximum likelihood analysis we ignore the contribution from lenses outside the field of view (e.g., Hudson et al. 1998). For small fields of view this tends to slightly lower the resulting halo masses and sizes. The area covered by our observations is much larger than the HDF North studied by Hudson et al. (1998), and the effect on our estimates is negligible.

To infer the best estimates for the model parameters, one formally has to perform a maximum likelihood analysis in which the redshift of each individual galaxy is a free parameter, which has to be chosen such that it maximizes the likelihood. This approach is computationally not feasible, and instead we create mock redshift catalogs,

using the observed redshift distributions from the CNOC2 survey (Hoekstra et al. 2003), which allows us to find estimates for the model parameters.

For each lens galaxy in the RCS catalog, with a given apparent  $R_C$  magnitude, we randomly draw a galaxy from the CNOC2 survey (with a similar  $R_C$ , but allowing for a small range in magnitude). The lens galaxy is then assigned the redshift and restframe  $B$ -band luminosity of that CNOC2 galaxy. We take the incompleteness of the survey into account when the redshifts are drawn from the survey. The mock catalogs are then analysed as if the redshifts of the lenses were known. Although this procedure does not provide the formal maximum likelihood parameter estimation, it does yield an unbiased estimate of the parameters. The procedure is repeated 10 times and enables us to properly account for the uncertainty introduced by the lack of precise redshifts for the lenses.

Future multi-color catalogs will improve the results presented here significantly. In particular, in the analysis presented here we have to adopt scaling relations between the velocity dispersion (or mass) and the luminosity of the lens and the extent of the halo and the luminosity. The use of photometric redshifts for the lenses will allow us to actually constrain these relations.

In §4.1 we consider the Truncated Isothermal Sphere (TIS; e.g., Brainerd et al. 1996; Schneider & Rix 1997; Hoekstra et al. 2003), which has been used previously in galaxy-galaxy lensing analyses. In §4.2 we compare the data to the popular NFW profile (Navarro et al. 1995, 1996, 1997).

#### 4.1. Truncated Isothermal Sphere Model

A simple model is the truncated isothermal sphere proposed by Brainerd et al. (1996). Its density profile is given by

$$\rho(r) = \frac{\sigma^2 s^2}{2\pi G r^2 (r^2 + s^2)}, \quad (2)$$

where  $\sigma$  is the line-of-sight velocity dispersion, and  $s$  is a truncation scale, i.e. the radius where the profile steepens. On small scales ( $r \ll s$ ) the model behaves as an Singular Isothermal Sphere (SIS) model, whereas for  $r \gg s$  the density decreases  $\propto r^{-4}$ . The mass contained within a sphere of radius  $r$  is given by

$$M(r) = \frac{2\sigma^2 s}{G} \arctan(r/s), \quad (3)$$

which results in a finite total mass of

$$M_{\text{tot}} = \frac{\pi\sigma^2}{G} s = 7.3 \times 10^{12} \left( \frac{\sigma}{100 \text{ km/s}} \right)^2 \left( \frac{s}{1 \text{ Mpc}} \right). \quad (4)$$

The projected surface density for this model is given by

$$\Sigma(r) = \frac{\sigma^2}{2Gr} \left( 1 - \frac{r}{\sqrt{r^2 + s^2}} \right). \quad (5)$$

The corresponding expressions for the shear can be found in Brainerd et al. (1996) and Schneider & Rix (1997).

We use this model to compute the model shear field and compare it to the data. The lenses, however, span a range in masses and we need to account for that using scaling

relations, which allow us to relate the halo properties of the lenses to those of a fiducial galaxy. For the fiducial galaxy we take a luminosity of  $L_B = 10^{10} h^{-2} L_{B\odot}$ .

Dynamical studies provide evidence of a power law scaling relation between the velocity dispersion and the luminosity (e.g., Tully-Fisher relation for spiral galaxies and Faber-Jackson relation for early type galaxies). We assume  $\sigma \propto L_B^{0.3}$ , which is based on the observed slope of the  $B$ -band Tully-Fisher relation (e.g., Verheijen 2001). Little is known, however, about the relation of the extent of dark matter halos with other (observable) parameters. Using SDSS data, Guzik & Seljak (2002) find that  $M \propto L_{g'}^{1.2 \pm 0.2}$ . Motivated by this result, we adopt  $s \propto L_B^{0.6}$ , which gives a total mass  $M \propto L_B^{1.2}$ . We note, however, that we probe lower luminosities than Guzik & Seljak (2002) (also see McKay et al. 2001) and as a result, the adopted scaling relation might differ from the actual ones.

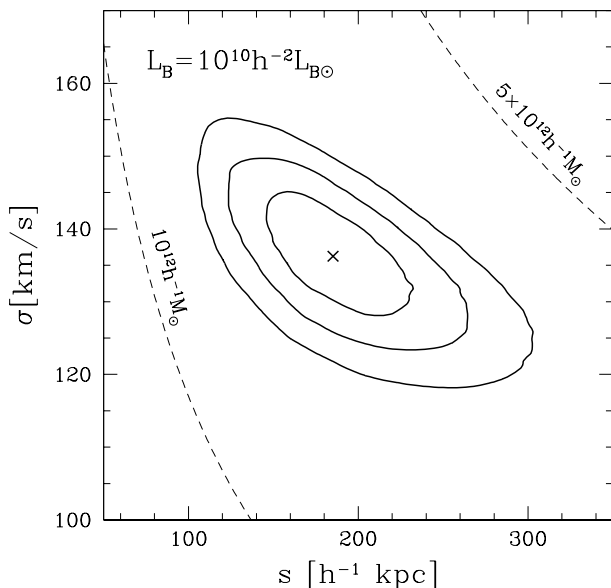


FIG. 3.— Joint constraints on the velocity dispersion  $\sigma$  and truncation parameter  $s$  for a fiducial galaxy with  $L_B = 10^{10} h^{-2} L_{B\odot}$ . The contours indicate the 68.3%, 95.4%, and the 99.7% confidence on two parameters jointly. The cross indicates the best fit value. The dashed lines indicate models with masses  $M_{\text{tot}} = 10 \times 10^{12} h^{-1} M_{\odot}$  and  $M_{200} = 5 \times 10^{12} h^{-1} M_{\odot}$ .

Figure 3 shows the joint constraints on the velocity dispersion  $\sigma$  and truncation parameter  $s$  for a fiducial galaxy with  $L_B = 10^{10} h^{-2} L_{B\odot}$ , under the assumption that the luminosity does not evolve with redshift. Conveniently, for this particular luminosity, the inferred values of the velocity dispersion and truncation parameter depend only marginally on the adopted scaling relations.

For the velocity dispersion we obtain a value of  $\sigma = 136 \pm 5 \pm 3$  km/s (68% confidence, marginalizing over all other model parameters). Hoekstra et al. (2003) find a velocity dispersion of  $\sigma = 110 \pm 12$  for a galaxy with a luminosity of  $5.6 \times 10^9 h^{-2} L_{B\odot}$ . For a galaxy with that luminosity, the adopted scaling relations imply a velocity dispersion of  $114 \pm 4 \pm 2$  km/s, in excellent agreement with Hoekstra et al. (2003). McKay et al. (2001) who found a best fit value of  $\sigma = 113_{-13}^{+17}$  km/s (95% confidence) for

a galaxy with  $L_{g'} \sim 9 \times 10^9 h^{-2} L_{g'\odot}$ . Our results correspond to a velocity dispersion of  $\sigma = 127 \pm 5 \pm 3$  km/s for a galaxy of that luminosity, in good agreement with the SDSS result.

We derive tight constraints on the truncation parameter, i.e. the extent of dark matter halos. We find a value of  $s = 185_{-28}^{+30} h^{-1}$  kpc (68% confidence), and a total mass  $M_{\text{tot}} = (2.5 \pm 0.3 \pm 0.1) \times 10^{12} h^{-1} M_{\odot}$ . The results presented in Hoekstra et al. (2003) imply a value of  $s = 290_{-82}^{+139} h^{-1}$  kpc (68% confidence) for their fiducial galaxy. For a galaxy with a luminosity of  $5.6 \times 10^9 h^{-2} L_{B\odot}$ , we obtain  $s = 131_{-20}^{+21} h^{-1}$  kpc, marginally consistent with Hoekstra et al. (2003).

If we assume that  $L_B \propto (1+z)$  we obtain a velocity dispersion of  $\sigma = 146 \pm 5 \pm 3$  km/s and a truncation size of  $s = 213_{-32}^{+35} h^{-1}$  kpc for a galaxy with  $L_B(z=0) = 10^{10} h^{-2} L_{B\odot}$ .

#### 4.2. NFW model

Numerical simulations of collisionless cold dark matter (CDM) reproduce the observed structure in the universe remarkably well. Furthermore these simulations suggest that CDM gives rise to a specific density profile, which fits the radial mass distribution for halos with a wide range in mass (e.g., Dubinski & Carlberg 1991; Navarro et al. 1995, 1996, 1997). The NFW density profile is characterized by 2 parameters, a density contrast  $\delta_c$  and a scale  $r_s$

$$\rho(r) = \frac{\delta_c \rho_c}{(r/r_s)(1+r/r_s)^2}, \quad (6)$$

where  $\rho_c$  is the critical surface density at the redshift of the halo. The “virial” radius  $r_{200}$  is defined as the radius where the mass density of the halo is equal to  $200\rho_c$ , and the corresponding mass  $M_{200}$  inside this radius is given by

$$M_{200} = \frac{800\pi}{3} \rho_c r_{200}^3, \quad (7)$$

with a corresponding rotation velocity  $V_{200}$  of

$$V_{200} = V(r_{200}) = \frac{GM_{200}}{r_{200}}. \quad (8)$$

The concentration parameter is defined as  $c = r_{200}/r_s$ , which yields an expression for the overdensity of the halo  $\delta_c$  in terms of  $c$

$$\delta_c = \frac{200}{3} \frac{c^3}{\ln(1+c) - c/(1+c)}. \quad (9)$$

It is important to note that the density profile on small scales remains controversial as other groups find different results (e.g., Moore et al. 1999; Ghigna et al. 2000). In addition, realistic simulations should include the effect of baryons, which complicate matters even further (see e.g., Mo, Mao & White 1998; Kochanek & White 2001). Unfortunately the current RCS data do not allow us to constrain the slope of the inner mass profile. However, future, deep lensing surveys, such as the CFHT Legacy Survey, will be well suited for such a study.

On the other hand, there is good agreement for the density profile on large scales, and a comparison of the profiles of real objects with the predictions provides an important

test of the assumption that structures form through dissipationless collapse. The predicted profiles agree well with the observed mass distribution in clusters of galaxies (e.g., Hoekstra et al. 2002d), but the situation is less clear for galaxy mass halos. Rotation curves can provide some constraints, but typical values for  $r_s$  for galaxy mass halos are  $10 - 20h^{-1}$  kpc, comparable to the outermost point for which rotation curves have been measured.

Galaxies that are thought to be dark matter dominated, such as low surface brightness galaxies, potentially might be more suitable to test the CDM predictions. Studies of the rotation curves of low surface brightness galaxies suggest that, at least for a fraction of them, the observed rotation curves rise more slowly than the CDM predictions (e.g. de Blok, McGaugh & Rubin 2001; McGaugh, Barker & de Blok 2002). It is not clear, however, whether such studies provide a good test of CDM, because low surface brightness galaxies are peculiar (Zwaan & Briggs 2000), and their formation is not well understood. Hence, it is not obvious that their halos should be described by an NFW profile. Recently Ricotti (2003) has suggested that the inner slope might depend on halo mass, with low mass systems having shallow cores, whereas massive galaxies are well described by the NFW profile.

In this section we compare the NFW profile to the observations, with  $\delta_c$  and  $r_s$  as free parameters. The equations describing the shear for the NFW profile have been derived by Bartelmann (1996) and Wright & Brainerd (2000).

As before we have to adopt scaling relations. We assume that the maximum rotation velocity scales  $\propto L_B^{0.3}$  (the B-band Tully-Fisher relation; Verheijen 2001). If we also assume that  $M_{200} \propto L_B^{1.2}$ , as motivated by the findings of Guzik & Seljak (2002), we obtain that  $r_s \propto L_B^{0.75}$  and  $\delta_c \propto L_B^{-0.85}$ .

Figure 4 shows the joint constraints on  $V_{200}$  and  $r_s$  for a galaxy with a luminosity of  $L_B = 10^{10}h^{-2}L_{B\odot}$ . In addition, the right axis indicates the corresponding values for  $M_{200}$ . We derive a best fit value of  $V_{200} = 162 \pm 5 \pm 3$  km/s, or  $M_{200} = (8.4 \pm 0.7 \pm 0.4) \times 10^{11}h^{-1}M_\odot$  (68% confidence), and a corresponding value of  $r_{200} = 139_{-5}^{+3}h^{-1}$  kpc. It is useful to compare this result with the mass from the TIS model.

The TIS model yields  $M_{\text{TIS}}(r_{200}) = (1.0 \pm 0.1) \times 10^{12}h^{-1}M_\odot$ , which is slightly larger than the NFW value. As shown by Wright & Brainerd (2000), isothermal models give higher masses compared to NFW models. Hence, the results derived from both models are consistent.

From their galaxy-galaxy lensing analysis of the SDSS, Guzik & Seljak (2002) find  $M_{200} = (9.3 \pm 1.6) \times 10^{11}h^{-1}M_\odot$  for a galaxy of  $L_{g'} \sim 1.1 \times 10^{10}h^{-2}L_{g'\odot}$ , in good agreement with our results.

For the scale  $r_s$  we find  $r_s = 16.2_{-2.9}^{+3.6}h^{-1}$  kpc (68% confidence), and the best fit density contrast is  $\delta_c = 2.4_{-0.8}^{+1.4} \times 10^4$  (68% confidence; confidence interval from Monte Carlo simulation). The TIS model provides a slightly better fit to the data, but the difference is not significant, and consequently the data are not sufficient to distinguish between the NFW and TIS model.

As before, we also calculated the results under the assumption that the luminosity evolves  $\propto (1+z)$ . In this case we find a value of  $r_s = 17.2_{-3.1}^{+3.8}h^{-1}$  kpc and  $V_{200} =$

$176 \pm 5 \pm 4$  km/s for a  $L_B(z=0) = 10^{10}h^{-2}L_{B\odot}$  galaxy.

In our maximum likelihood analysis we considered  $r_s$  and  $V_{200}$  (or equivalently the mass  $M_{200}$ ) as free parameters. Numerical simulations of CDM, however, show that the parameters in the NFW model are correlated, albeit with some scatter. As a result, the NFW model can be considered as a one-parameter model: given the cosmology, redshift, and one of the NFW parameters, the values for all other parameters can be computed using the routine CHARDEN made available by Julio Navarro<sup>1</sup>. Hence, the simulations make a definite prediction for the value of  $V_{200}$  as a function of  $r_s$ . The dotted line in Figure 4 indicates this prediction. If the simulations provide a good description of dark matter halos, the dotted line should intersect our confidence region, which it does.

This result provides important support for the CDM paradigm, as it predicts the correct ‘‘size’’ of dark matter halos. It is important to note that this analysis is a direct test of CDM (albeit not conclusive), because the weak lensing results are inferred from the gravitational potential at large distances from the galaxy center, where dark matter dominates. Most other attempts to test CDM are confined to the inner regions, where baryons are, or might be, important.

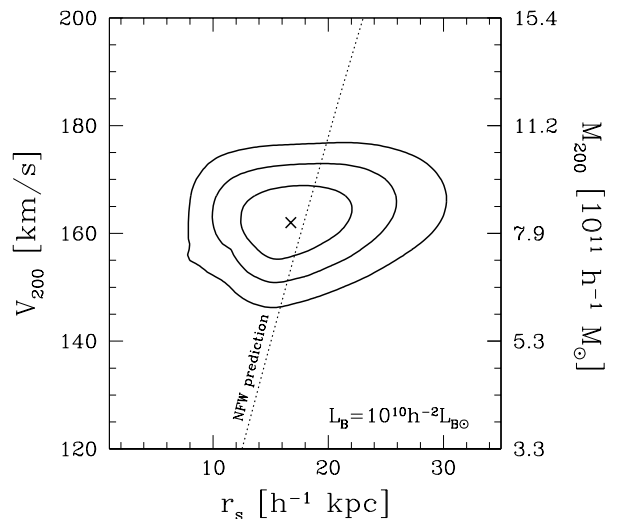


FIG. 4.— Joint constraints on  $\delta_c r_s^2$  and scale radius  $r_s$  for a fiducial galaxy with  $L_B = 10^{10}h^{-2}L_{B\odot}$ , with an NFW profile. The contours indicate the 68.3%, 95.4%, and the 99.7% confidence on two parameters jointly. The cross indicates the best fit value. The dashed lines indicate models with masses  $M_{200} = 5 \times 10^{11}h^{-1}M_\odot$  and  $M_{200} = 10^{12}h^{-1}M_\odot$ . The dotted line indicates the predictions from the numerical simulations, which are in excellent agreement with our results.

## 5. SHAPES OF HALOS

The average shape of dark matter halos can provide important information about the nature of dark matter. Numerical simulations of cold dark matter yield triaxial halos, with a typical ellipticity of  $\sim 0.3$  (e.g., Dubinski &

<sup>1</sup> The routine CHARDEN can be obtained from <http://pinot.phys.uvic.ca/~jfn/charden>

Carlberg 1991). Hence, in the context of collisionless cold dark matter, the theoretical evidence for flattened halos is quite strong. If the dark matter is interacting, it tends to produce halos that are more spherical (compared to cold dark matter). This difference is more pronounced in the central parts of the halo, where the density is high. On the large scales probed by weak lensing, the different types of dark matter (for reasonable interaction cross-sections) produces halos with similar shapes.

Nevertheless, a measurement of the average shape of dark matter halos is important, because the observational evidence is still limited. Dynamical measurements are limited by the lack of visible tracers, and therefore only probe the vertical potential on scales  $\leq 15$  kpc. Although the spread in inferred values for the axis ratio  $c/a$  (where  $c/a$  is the ratio of the shortest to longest principle axis of the halo) is large, the results suggest an average value of  $c/a = 0.5 \pm 0.2$  (Sackett 1999).

Weak gravitational lensing is potentially the most powerful way to derive constraints on the shapes of dark matter halos. The amount of data required for such a measurement, however, is large (e.g., Brainerd & Wright 2000; Natarajan & Refregier 2000): the galaxy-galaxy lensing signal is small, and now one needs to measure an even smaller azimuthal variation. We also have to assume that the galaxy and its halo are aligned. An imperfect alignment between light and halo will reduce the amplitude of the azimuthal variation detectable in the weak lensing analysis. Hence, weak lensing formally provides a lower limit to the average halo ellipticity.

Brainerd & Wright (2000) and Natarajan & Refregier (2000) proposed to study the azimuthal variation in the tangential shear around the lenses. On very small scales, the lensing signal is dominated by the lens, but on larger scales, the clustering of the lenses will lower the signal one tries to measure (the two point function is axisymmetric). We therefore use the maximum likelihood approach used in the previous section.

To maximize the signal-to-noise ratio of the measurement one has to assign proper weights to the lenses: edge-on galaxies have maximal weight, whereas the lensing signal around face-on galaxies contains no information about the shape of the halo. We adopt a simple approach, and assume that the (projected) ellipticity of the dark matter halo is proportional to the shape of the galaxy:  $e_{\text{halo}} = f e_{\text{lens}}$ .

The measurement of the azimuthally averaged tangential shear around galaxies is robust against residual systematics (e.g., imperfect correction for PSF anisotropy): contributions from a constant or gradient residual shear cancel. This is no longer the case for the quadrupole signal, and imperfect correction for the PSF anisotropy can mimic the signal from a flattened halo.

If the lens galaxy is oriented randomly with respect to the residual shear, the average over many lenses will cancel the contribution from systematics. In real data, however, the uncorrected shapes of the lenses are aligned with the systematic signal. Hence, an imperfect correction can give rise to a small quadrupole signal, although we note that the lenses used in our analysis are large compared to the PSF. We estimate the amplitude of this effect in Appendix A, and show that it is negligible for the measure-

ments presented here. We also examined the robustness of our results by splitting the data into two samples and comparing the results.

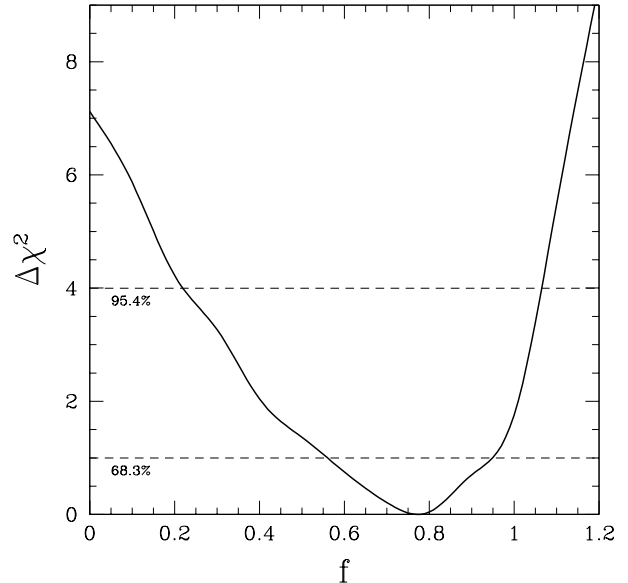


FIG. 5.—  $\Delta\chi^2$  as a function of  $f$ . We have assumed that the ellipticity of the halos is related to the observed ellipticity of the lens as  $e_{\text{halo}} = f e_{\text{lens}}$ . We have indicated the 68.3% and 95.4% confidence intervals. We find a best fit value of  $f = 0.77^{+0.18}_{-0.21}$  (68% confidence). Round halos ( $f = 0$ ) are excluded with 99.5% confidence.

We use an elliptical TIS model to compute the model shear field, and compare this to the data. Figure 5 shows the resulting  $\Delta\chi^2$  as a function of  $f$ . We find a best fit value of  $f = 0.77^{+0.18}_{-0.21}$  (68% confidence). This suggests that, on average, the dark matter distribution is rounder than the light distribution. As discussed above, our analysis formally provides only a lower limit on the halo ellipticity, and the true ellipticity might be higher if some of the halos are misaligned with the light. Nevertheless, the fact that we detect a significant flattening implies that the halos are well aligned with the light distribution. Also note that the lensing signal is caused by a range of different galaxy types, for which our simple relation between the halo ellipticity and light distribution might not be valid.

Consequently the interpretation of the results is difficult, although a simple interpretation actually yields sensible results. For instance, the average ellipticity of the lens galaxies is  $\langle e_{\text{lens}} \rangle = 0.414$ . Hence, the measured value of  $f$  implies an average projected halo ellipticity of  $\langle e_{\text{halo}} \rangle = 0.33^{+0.07}_{-0.09}$  (68% confidence), which corresponds to an projected axis ratio of  $c/a = 0.67^{+0.09}_{-0.07}$  (68% confidence; where we have used  $c/a = 1 - e$ ). Although the weak lensing yields a projected axis ratio, the result is in fair agreement with the results from numerical simulations.

A robust outcome of our analysis is that spherical halos ( $f = 0$ ) are excluded with 99.5% confidence. As we demonstrate below, this poses serious problems for alternative theories of gravity, which attempt to explain the observations without dark matter.



### 5.1. Implications for alternative theories of gravity

In this section we examine the implications of our measurement of the anisotropy in the lensing signal around galaxies for theories of gravity without dark matter. We focus on one particular approach: Modified Newtonian Dynamics (MOND; Milgrom 1983; Sanders 1986; Sanders & McGaugh 2002), which has been shown to describe rotation curves rather well (e.g., Begeman et al. 1991; Sanders & Verheijen 1998).

In principle weak lensing can be used as a powerful test of MOND, but unfortunately no relativistic description of MOND has been found. Consequently one cannot compute the lensing signal in this theory. However, even in the absence of an appropriate description of lensing, we can use the observed anisotropy in the lensing signal around galaxies to test MOND.

In any reasonable alternative theory of gravity, the anisotropy in the lensing signal of an *isolated* galaxy is caused by the distribution of light and gas in that galaxy. In order to explain the flat rotation curves, these alternative theories typically need an effective force law  $\propto r^{-1}$ . Hence, on small scales one expects an anisotropic signal, but at large radii (where there are no stars and gas) we assume that the anisotropy in the lensing signal decreases  $\propto r^{-2}$ . As a result, these theories predict an almost isotropic weak lensing signal on the scales probed by our analysis, which is not observed.

Galaxies, however, are not isolated and the external field effect (Milgrom 1986) might complicate the interpretation of our measurements. In MOND, if a galaxy is embedded in an external field, this field dominates the dynamics if its acceleration is larger than the acceleration of the galaxy. As a result, the effective gravitational field is non-spherical, even if the potential of the galaxy is isotropic (as is the case for an isolated galaxy).

This effect is important if galaxies would be aligned with this external field. We know, however, that the intrinsic alignments of galaxies are small (e.g., Lee & Pen 2001, 2002) and for the measurements presented here, it is safe to assume that the lenses have random orientation with respect to any external field. Consequently, the observed anisotropy in the lensing signal cannot be caused by the external field effect.

Hence, our findings provide strong support for the existence of dark matter, because alternative theories of grav-

ity predict an almost isotropic lensing signal. Better constraints can be derived from future weak lensing surveys, which will allow us to study the anisotropy a function of projected distance from the galaxy.

## 6. CONCLUSIONS

We have analysed the weak lensing signal caused by a sample of lenses with  $19.5 < R_C < 21$  using  $45.5 \text{ deg}^2$  of  $R_C$  band imaging data from the Red-Sequence Cluster Survey (RCS). We have studied the average mass profile around the lenses using a maximum likelihood analysis. To this end, we considered two models for the halo mass profile: a truncated isothermal sphere and an NFW profile. We have assumed (observationally motivated) scaling relations between the luminosity of the lens and the velocity dispersion and the extent of the halo.

The TIS model yields a best fit velocity dispersion of  $\sigma = 136 \pm 5 \pm 4 \text{ km/s}$  and a truncation radius  $s = 185_{-28}^{+30} h^{-1} \text{ kpc}$  for a galaxy with a fiducial luminosity of  $L_B = 10^{10} h^{-2} L_{B\odot}$ . Alternatively, the best fit NFW model yields a mass  $M_{200} = (8.4 \pm 0.7 \pm 4) \times 10^{11} h^{-1} M_\odot$  and a scale radius  $r_s = 16.2_{-2.9}^{+3.6} h^{-1} \text{ kpc}$ . This value for the scale radius is in excellent agreement with predictions from numerical simulations for a halo of this mass.

We also present the first detection of the flattening of galaxy dark matter halos from weak lensing. We use a simple model in which the ellipticity of the halo is  $f$  times the observed ellipticity of the lens. We find a best fit value of  $f = 0.77_{-0.21}^{+0.18}$  (68% confidence), suggesting that the dark matter halos are somewhat rounder than the light distribution. The fact that we detect a significant flattening implies that the halos are aligned with the light distribution. Given the average ellipticity of the lenses, this implies a halo ellipticity of  $\langle e_{\text{halo}} \rangle = 0.33_{-0.09}^{+0.07}$  (68% confidence), in fair agreement with results from numerical simulations of CDM. This result provides strong support for the existence of dark matter, as an isotropic lensing signal is excluded with 99.5% confidence.

We are grateful to the anonymous referee whose comments have significantly improved the quality of this paper. The RCS project is partially supported by grants from the Natural Science and Engineering Science Council of Canada and the University of Toronto to HKCY.

## APPENDIX

### CONTRIBUTION OF SYSTEMATICS TO THE SHAPE MEASUREMENT OF DARK HALOS

In this appendix we examine how residual systematics affect the measurement of the flattening of dark matter halos. A schematic overview of the situation is presented in Figure A6. The thin lines indicate the direction of residual systematics. The residual shear has an amplitude  $\hat{\gamma}$  and a position angle  $\phi$  with respect to the major axis of the lens. The tangential shear  $\gamma_T^{\text{obs}}$  observed at a position  $(r, \theta)$  is the sum of the lensing signal  $\gamma_T^{\text{lens}}$  and the contribution from systematics  $\hat{\gamma}_T$ . The latter is given by

$$\hat{\gamma}_T = -\hat{\gamma}[\cos(2\phi)\cos(2\theta) + \sin(2\phi)\sin(2\theta)] = -\hat{\gamma}\cos(2(\theta - \phi)). \quad (\text{A1})$$

Hence, the azimuthally averaged tangential shear is not affected by systematics as  $\int d\theta \hat{\gamma}_T(\theta) = 0$ , and the weak lensing mass estimate is very robust. For a flattened halo, the lensing signal  $\gamma_T^{\text{lens}}$  is given by

$$\gamma_T^{\text{lens}}(r, \theta) = [1 + \gamma_f \cos(2\theta)] \cdot \langle \gamma_T \rangle(r), \quad (\text{A2})$$

where  $\langle \gamma_T \rangle$  is the azimuthally averaged tangential shear, and  $\gamma_f$  is a measure of the flattening of the halo. For positive values of  $\gamma_f$ , the halo is aligned with the lens.

We consider the worst case scenario, and demonstrate that even in this situation the results are robust. One way to estimate the flattening of the halo is to measure the shears  $\gamma_+$  (at  $\theta = 0$  and  $\pi$ ), and  $\gamma_-$  (at  $\theta = \pi/2$  and  $3\pi/2$ ). The observed ratio  $f = \gamma_-/\gamma_+$  is

$$f_{\text{obs}} = \frac{\gamma_- + \hat{\gamma} \cos(2\phi)}{\gamma_+ - \hat{\gamma} \cos(2\phi)}. \quad (\text{A3})$$

If  $\phi$  is uncorrelated with the lens, the observed ratio, averaged over many lenses, is unaffected by systematics because  $\langle \cos(2\phi) \rangle = 0$ . However, in real data, the PSF anisotropy affects both the lens and the source galaxies. Although the lenses used in this paper are large compared to the PSF, any (small) residual in the correction will introduce a correlation in the position angle of the lens and the direction of the PSF anisotropy.

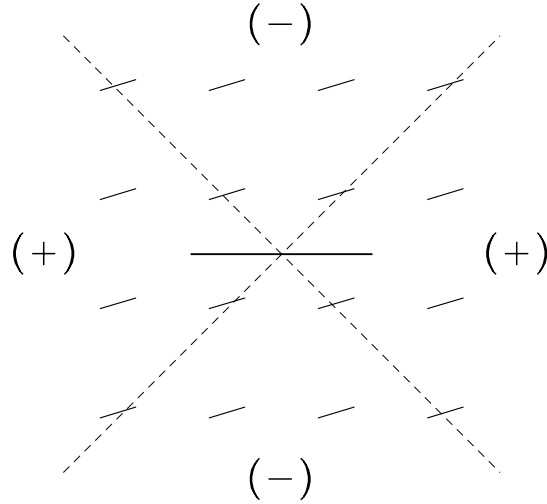


FIG. A6.— Schematic view of the lens galaxy and the residual systematic shear. If the dark halo is flattened and aligned with the lens (line in the center) then the tangential shear at a given radius is larger in the quadrants indicated by (+), and lower in (-). The small lines indicate the direction of the residual shear (e.g., caused by the imperfect correction for PSF anisotropy). The residual shear has an amplitude  $\hat{\gamma}$  and has a direction with a position angle  $\phi'$  with respect to the lens.

The effect is maximal for  $\phi = 0$  (aligned with the major axis of the lens) or  $\phi = \pi/2$  (perpendicular to major axis of the lens). The latter situation corresponds to an overcorrection of the PSF anisotropy, whereas the former occurs when the correction for PSF anisotropy is too small. For both (extreme) situations, only the observed value of  $\gamma_1$  is affected by systematics ( $\gamma_2$  is left unchanged). The observed value  $\gamma_1^{\text{obs}}$  for the lens can be written as  $\gamma_1^{\text{obs}} = \gamma_1^{\text{true}} + \alpha\hat{\gamma}$ , where  $\alpha$  is a measure of the correlation between the position angle of the lens and the direction of the systematic shear of the background galaxies. In our case  $\alpha \ll 1$ , because the lenses are large compared compared to the PSF. For a lens with with an observed  $\gamma = \sqrt{\gamma_1^2 + \gamma_2^2}$ , we find

$$\langle \cos(2\phi) \rangle = \frac{\alpha\hat{\gamma}}{2\gamma}. \quad (\text{A4})$$

The distribution of  $\gamma_1$  and  $\gamma_2$  can be approximated by a Gaussian with a dispersion  $\sigma$  (with a typical value of  $\sigma = 0.2$ ). For the ensemble of lenses we then obtain

$$\langle \cos(2\phi) \rangle = \sqrt{\frac{\pi}{2}} \frac{\alpha\hat{\gamma}}{2\sigma}. \quad (\text{A5})$$

This introduces a relatively large signal because face-on lenses ( $\gamma \approx 0$ ) align easily with the PSF anisotropy. Such lenses, however, contain no information about the shape of the halo. In our analysis we assign a weight  $\propto \gamma$  to each lens. Hence in our case we are less sensitive to systematics as the correct estimate is given by

$$\langle \cos(2\phi) \rangle = \frac{\alpha\hat{\gamma}}{2}. \quad (\text{A6})$$

Hence, the observed ratio  $\gamma_-/\gamma_+$  reduces to

$$f_{\text{obs}} = \frac{\gamma_- + \hat{\gamma}^2 \alpha / 2}{\gamma_+ - \hat{\gamma}^2 \alpha / 2} \quad (\text{A7})$$

We can now estimate how robust the measurement of the average halo shape is. We take a conservative estimate of  $\alpha = 0.5$ , and  $\hat{\gamma} = 5 \times 10^{-3}$  (see Hoekstra et al. 2002a for a discussion of the residuals in our data). The average separation of stars in our data is  $\sim 1.5$  and therefore the residual PSF anisotropy is likely to change direction on scales larger than the separation of the stars used to measure the anisotropy. The average tangential shear at 2 arcminutes is  $\sim 5 \times 10^{-4}$ . For a spherical halo ( $\gamma_- = \gamma_+ = 5 \times 10^{-4}$ ) we would observe a ratio  $f_{\text{obs}} = 1.025$ . This corresponds to an ellipticity of 2.5% (with the halo oriented perpendicular to the lens), which is small ( $\sim 10\%$  of the observed ellipticity).

In this very conservative estimate, we have assumed that for each lens, the residual PSF anisotropy is aligned with the lens (i.e., the PSF anisotropy was underestimated). There is, however, an equal probability of overestimating the PSF anisotropy. Hence, the estimate is a very conservative upper limit for the importance of systematics. Such a systematic underestimate for PSF anisotropy would give rise to very large ‘‘E’’ and ‘‘B’’-modes in the cosmic shear measurements, which are not observed. Hence, in reality the change in the ellipticity of the halo, caused by systematics, is much smaller than our conservative estimate.

#### REFERENCES

- Bartelmann, M. 1996, *A&A*, 313, 697  
 Begeman, K.G., Broeils, A.H., & Sanders, R.H. 1991, *MNRAS*, 249, 523  
 Bernstein, G.M. & Norberg, P. 2002, *AJ*, 124, 733  
 Brainerd, T.G., Blandford, R.D., & Smail, I. 1996, *ApJ*, 466, 623  
 Brainerd, T.G. & Wright, C.O. 2000, *astro-ph/0006281*  
 Carlberg, R.G., Yee, H.C., & Ellingson 1997, *ApJ*, 478, 462  
 Cohen, J.G. et al. 2000, *ApJ*, 538, 29  
 de Blok, W.J.G., McGaugh, S.S. & Rubin, V.C. 2001, *AJ*, 122, 2396  
 Dell’Antonio, L.P., & Tyson, J.A. 1996, *ApJ*, 473, L17  
 Dubinski, J. & Carlberg, R.G. 1991, *ApJ*, 378, 496  
 Fischer, P., et al. 2000, *AJ*, 120, 1198  
 Fernández-Soto, A., Lanzetta, K.M., & Yahil, A. 1999, *ApJ*, 513, 34  
 Ghigna, S., Moore, B., Governato, F., Lake, G., Quinn, T. Stadel, J. 2000, *ApJ*, 544, 616  
 Griffiths, R.E., Casertano, S., Im, M., & Ratnatunga, K.U. 1996, *MNRAS*, 282, 1159  
 Gladders, M.D. & Yee, H.K.C. 2003, to be submitted to *ApJS*  
 Guzik, J., & Seljak, U. 2001, *MNRAS*, 321, 439  
 Guzik, J., & Seljak, U. 2002, *MNRAS*, 335, 311  
 Hoekstra, H., Franx, M., Kuijken, K., & Squires, G. 1998, *ApJ*, 504, 636  
 Hoekstra, H., Yee, H.K.C., & Gladders, M.D. 2001b, *ApJ*, 558, L11  
 Hoekstra, H., Yee, H.K.C., Gladders, M.D., Barrientos, L.F., Hall, P.B., & Infante, L. 2002a, *ApJ*, 572, 55  
 Hoekstra, H., Yee, H.K.C., & Gladders, M.D. 2002b, *ApJ*, 577, 595  
 Hoekstra, H., van Waerbeke, L., Gladders, M.D., Mellier, Y., & Yee, H.K.C. 2002c, *ApJ*, 577, 604  
 Hoekstra, H., Franx, M., Kuijken, K., & van Dokkum, P.G. 2002d, *MNRAS*, 333, 911  
 Hoekstra, H., Franx, M., Kuijken, K., Carlberg, R.G., & Yee, H.K.C. 2003, *MNRAS*, 340, 609  
 Hudson, M.J., Gwyn, S.D.J., Dahle, H., & Kaiser, N. 1998, *ApJ*, 503, 531  
 Kauffmann, G., Colberg, J.M., Diaferio, A., White, S.D.M. 1999a, *MNRAS*, 303, 188  
 Kauffmann, G., Colberg, J.M., Diaferio, A., White, S.D.M. 1999b, *MNRAS*, 307, 529  
 Keeton, C.R., Kochanek, C.S., & Falco, E.E. 1998, *ApJ*, 509, 561  
 Kochanek, C.S., & White, M. 2001, *ApJ*, 559, 531  
 Lee, J. & Pen, U.-L. 2001, *ApJ*, 555, 106  
 Lee, J. & Pen, U.-L. 2001, *ApJ*, 567, L111  
 Lin, H., Yee, H.K.C., Carlberg, R.G., Morris, S.L., Sawicky, M., Patton, D.R., Wirth, G., & Shepherd, C.W. 1999, *ApJ*, 518, 533  
 McGaugh, S.S., Barker, M.K. & de Blok, W.J.G. 2002, *astro-ph/0210641*  
 McKay, T.A., et al. 2001, *ApJ*, submitted, *astro-ph/0108013*  
 McKay, T.A., et al. 2002, *ApJ*, 571, L85  
 Milgrom, M. 1983, *ApJ*, 270, 365  
 Milgrom, M. 1986, *ApJ*, 302, 617  
 Mo, H.J., Mao, S., & White, S.D.M. 1998, *MNRAS*, 295, 319  
 Moore, B., Quinn, T., Governato, F., Stadel, J., & Lake, G. 1999, *MNRAS*, 310, 1147  
 Natarajan, P. & Refregier, A. 2000, *ApJ*, 538, L113  
 Navarro, J.F., Frenk, C.S., & White, S.D.M. 1995, *MNRAS*, 275, 56  
 Navarro, J.F., Frenk, C.S., & White, S.D.M. 1996, *ApJ*, 462, 563  
 Navarro, J.F., Frenk, C.S., & White, S.D.M. 1997, *ApJ*, 490, 493  
 Prada, F., et al. 2003, *ApJ*, submitted, *astro-ph/0301360*  
 Ricotti, M. 2003, *MNRAS*, submitted, *astro-ph/0212146*  
 Sackett, P. 1999 in *Galaxy Dynamics*, ASP Conf. Series 182, eds. D.R. Merritt, M. Valluri, & J.A. Sellwood  
 Sanders, R.H., & McGaugh, S.S. 2002, *ARA&A*, 40, 263  
 Sanders, R.H., & Verheijen, M.A.W. 1998, *ApJ*, 503, 97  
 Sanders, R.H. 1986, *MNRAS*, 223, 539  
 Schneider, P., & Rix, H.-W. 1997, *ApJ*, 474, 25  
 Seljak, U. 2002, *MNRAS*, 334, 797  
 Smith, D.R., Bernstein, G.M., Fischer, P., & Jarvis, M. 2001, *ApJ*, 551, 643  
 Tyson, J.A., Valdes, F., Jarvis, J.F., & Mills, A.P., Jr. 1984 *ApJ*, 281, L59  
 van Albada, T.S., & Sancisi, R. 1986, *Phil. Trans. Roy. Soc., London*, A320, 447  
 Verheijen, M.A.W. 2001, *ApJ*, 563, 694  
 Wilson, G., Kaiser, N., Luppino, G.A., Cowie, L.L. 2001, *ApJ*, 555, 572  
 Wright, C.O. & Brainerd, T.G. 2000, *ApJ*, 534, 34  
 Yee, H.K.C., et al. 2000, *ApJS*, 129, 475  
 Yee, H.K.C., & Gladders, M.D. 2001, in ‘‘AMiBA 2001: High-z Clusters, Missing Baryons, and CMB Polarization’’, ASP Conference Series, Eds. L.-W. Chen et al., *astro-ph/0111431*  
 Zaritsky, D., & White, S.D.M. 1994, *ApJ*, 435, 599  
 Zwaan, M.A. & Briggs, F.H. 2000, *ApJ*, 530, 61